基于变参数坡口模型分层焊材消耗计算

沈春龙[1]， 钱晓军[1]， 黄有仁[1]， 王克鸿[2]
（1. 南京师范大学 计算机系，南京 210097；2. 南京理工大学 材料科学与工程系，南京 210094）

摘 要：焊材消耗用量计算是焊接工艺设计的重要内容. 在双边双面 U 形坡口参数描述的基础上，改变参数演变为其它常见类型坡口，实现常见坡口类型统一化参数模型，便于焊缝截面面积计算. 通过对该模型焊缝横截面分解，将复杂截面面积求解简化为简单图形面积计算，计算各焊接工序焊材消耗用量必须求解对应焊层横截面面积，提出了焊层截面面积计算思想并给出基于焊层厚度横截面面积计算理论，在此基础上设计了分层的迭代计算算法并开发了软件计算工具，说明了软件使用方法，测试计算了一个实际坡口焊材用量. 结果表明，能够显著提高焊材计算精度和效率.

关键词：焊材消耗用量；焊接工艺；参数模型；焊层面积
中图分类号：TG319.72 文献标识码：A 文章编号：0253－360X(2009)03－0033－04

沈春龙

0 序 言

在传统的焊接工艺设计过程中，除了设计焊接工艺参数外，焊缝焊材计算和产品焊材汇总也是一个重要内容. 由于坡口形式的多样性和不规则性，导致焊缝截面面积较难计算；另一方面，在焊接过程中存在不同焊接方法和所使用焊材的不一致，需要计算各焊层截面面积. 这两方面使得焊材分类用量计算较为繁琐. 目前工艺设计人员计算焊材用量主要采用两种方式：一种是根据经验公式，利用计算器粗略计算焊层面积来计算焊材用量；另一种是直接查找经验表，直接获得焊材质量. 这两种方式的直接结果是效率低，计算结果误差较大，导致焊材浪费，产品制造成本加大[1,2]. 通过变参数模型来统一描述坡口形状，设计焊材用量理论计算方法，提出基于焊层厚度递推计算焊层截面面积的算法，使得焊材用量计算工具化，计算精度和效率显著提高，达到“甩计算器”的目的. 上述模型及算法已用于开发的承压设备焊接工艺辅助设计网络版 Net _WCAPP 软件中[3]，已在多家压力容器制造单位使用，实践表明能够有效提高计算精度和效率.

1 基于变参数坡口形状模型

如图 1 所示，以双边双面对称 U 形坡口模型为例，E 为坡口单双边系数，$E=2$ 为双边坡口，$E=1$ 为单边坡口，设上坡口为先焊面，下坡口为后焊面，h 为后焊面的坡口深度，$h=0$ 表示坡口为单面，δ 为整个坡口厚度，α_1，α_2 分别为上下坡口角度，R_1，R_2 为上下坡口半径，P 为钝边高度，C 为组对间隙. 一些常见的单、双面、对称坡口形式可以随双边坡口形状参数变化演变而来. 图 1a 为在双边双面对称 U 形坡口，当参数变化时演变为双边单面 U 形坡口图 1b，该模型为坡口形状参数化表示及后续焊材用量计算理论分析与设计提供依据.

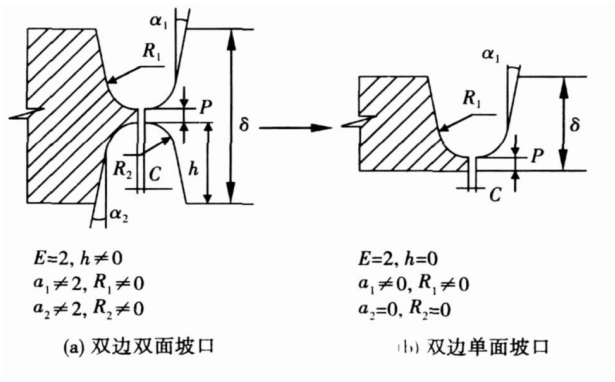

图 1 双边双面 U 形坡口变参数模型

Fig. 1 Variant parameter model of double U groove

2 焊缝横截面面积计算理论分析

2.1 坡口焊缝横截面表示

以双边双面 U 形坡口焊缝为例，焊缝截面如图

收稿日期：2008－01－28
基金项目：国家自然科学基金资助项目(编号 60875001)；国防基础科研基金资助项目(编号 B2620080137)

2 所示，将焊缝横截面面积分解成四个部分：坡口面积 S_p，间隙面积 S_c，焊缝余高面积 S_e 及清根焊缝面积 S_g，整体横截面面积 $S = S_p + S_c + S_e + S_g$；当坡口为双面时，$S_p = S_{p1} + S_{p2}$；$S_c = S_{c1} + S_{c2}$；$S_e = S_{e1} + S_{e2}$. 分解的目的是通过计算四个局部单元面积来计算整体截面面积. 间隙横截面面积 $S_c =$ ∂C；清根截面面积计算采用近似公式 $S_g = 0.75 g_w \cdot g_h$，g_w，g_h 分别为清根宽度和清根高度.

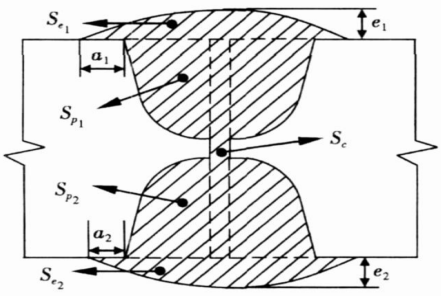

图 2 U 形坡口焊缝截面示意图

Fig. 2 Weld cross-section of U groove

2.2 多工序焊缝焊层截面面积求解理论

在接头坡口施焊时，通常采用多种焊接工序完成，对各个工序都需要计算焊材用量. 将焊缝面积分为先、后部分面积，设先焊面横截面面积 S_f，后焊部分横截面面积 S_s，则整个焊缝面积 $S = S_f + S_s$. 对单面焊而言 $S = S_f$，S_f，S_s 为先后焊面若干层工序横截面面积之和.

设先焊面有 n_1 个焊层，第 i 层焊接工序的焊缝厚度为 $\Delta \delta_{fi}$，横截面积为 ΔS_{fi}，S_{fi} 为从基准到第 i 层总截面面积，基准选在钝边下沿线，δ_{fi} 为从钝边上沿线到第 i 层的厚度，S_f 为先焊面的总面积；后焊面有 n_2 个焊层，第 i 层焊接工序的焊缝厚度为 $\Delta \delta_{si}$，横截面积为 ΔS_{si}，S_{si} 为从基准到第 i 层总截面面积，δ_{si} 为从基准到第 i 层的厚度，S_s 为后焊面的总面积.

以双面对称U形坡口先焊面为例，各参数如图3所示. 计算焊层截面面积 ΔS_{fi} 是模型建立的目标.

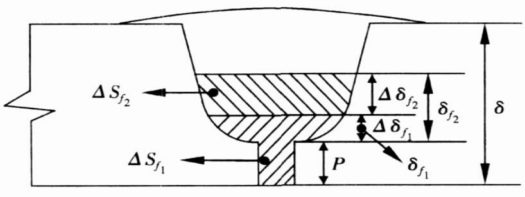

图 3 分层计算参数模型

Fig. 3 Layered parameter model

其求解的思想是先计算从第一层到第 i 层整个截面面积 S_{fi}，然后减去前 $i-1$ 层截面总面积 S_{fi-1}，即 $\Delta S_f i = S_{fi} - S_{i-1}$，对第 i 层截面面积计算而言，需要利用前一步的历史计算数据 S_{fi-1}，提高了截面积的计算效率. 焊层截面面积计算的理论设计分析如下.

(1) 先后焊面的总面积 S_s，S_f 表达式为

$$\left.\begin{aligned} S_f &= \sum_{i=1}^{n1} \Delta S_{fi} = \Delta S_{f1} + \cdots \Delta S_{fn1} \\ S_s &= \sum_{i=1}^{n2} \Delta S_{si} = \Delta S_{s1} + \cdots \Delta S_{sn2} \end{aligned}\right\} \tag{1}$$

(2) 先焊面每层截面积 ΔS_{fi} 与第 i 层的总面积 S_{fi} 之间的迭代关系表达式为

$$\left.\begin{aligned} \Delta S_{f1} &= S_{f1} \\ \Delta S_{f2} &= S_{f2} - S_{f1} \\ &\cdots\cdots \\ \Delta S_{fn1} &= S_{fn1} - S_{fn1-1} \\ \Delta S_{fn1} &= \Delta S_{fn1} + S_{e1} \end{aligned}\right\} \tag{2}$$

$$S_{e1} = \frac{3}{4}[\, Ea_1 + ER_1 + C + E\mathrm{tg}\alpha_1 \quad (\delta - P - R_1 - h)\,]\, e_1 \tag{3}$$

后焊面每层截面积 ΔS_{si} 与第 i 层的总面积 S_{si} 之间的迭代关系，通常将清根面积加到后焊面的第一层，其表达式为

$$\left.\begin{aligned} \Delta S_{s1} &= S_{s1} + S_g \\ \Delta S_{s2} &= S_{s2} - S_{s1} \\ &\cdots\cdots \\ \Delta S_{sn2} &= S_{sn2} - S_{sn2-1} \\ \Delta S_{sn2} &= \Delta S_{sn2} + S_{e2} \end{aligned}\right\} \tag{4}$$

$$S_{e2} = \frac{3}{4}[\, Ea_2 + ER_2 + C + (h - R_2)\mathrm{tg}\alpha_2\,]\, e_2 \tag{5}$$

(3) 先焊面第 i 层的总面积 S_{fi} 的计算过程

考虑到 U 形坡口形状，分两种情况计算，当 $\delta_{fi} < R_1$ 时，将焊缝截面分为两个部分：弓形和矩形，计算结果为

$$S_{fi} = \frac{3}{4} E \frac{1}{2} \sqrt{2\delta_{fi} R_1 - \delta_{fi}^2}\, \delta_{fi} + (P + \delta_{fi}) C \tag{6}$$

当 $\delta_{fi} \geqslant R_1$ 时，焊缝截面分为四个部分：半圆、两个矩形和一个三角形，计算结果为

$$S_{fi} = \frac{\pi R^2}{4} E + \frac{E}{2} (\delta_{fi} - R_1)^2 \mathrm{tg}\alpha_1 + ER_1 \quad (\delta_{fi} - R_1) + (\delta_{fi} + P) C \tag{7}$$

后焊面第 i 层的总面积 S_{si} 的计算同样分两种情况计算，当 $\delta_{si} < R_2$ 时，表达式为

$$S_{si} = \frac{3}{4} E \frac{1}{2} \sqrt{2\delta_{si} R_2 - \delta_{si}^2}\, \delta_{si} + \delta_{si} C \tag{8}$$

当 $\delta_{si} \geqslant R_2$ 时, 表达式为

$$S_{si} = \frac{\pi R^2}{4}E + \frac{E}{2}(\delta_{si} - R_2)^2 \mathrm{tg}\,\alpha_2 + E(\delta_{si} - R_2)R_2 + \delta_{si}C \tag{9}$$

先焊面 i 层总厚度 δ_{fi} 与第 i 焊层厚度 $\Delta\delta_{fi}$ 为

$$\left.\begin{aligned}\delta_{fn1} &= \sum_{i=1}^{n1}\Delta\delta_{fi}\\ \delta_{f1} &= \Delta\delta_{f1}\end{aligned}\right\} \tag{10}$$

后焊面 i 层总厚度 δ_{si} 与第 i 焊层厚度 $\Delta\delta_{si}$ 关系为

$$\left.\begin{aligned}\delta_{sn2} &= \sum_{i=1}^{n2}\Delta\delta_{si}\\ \delta_{s1} &= \Delta\delta_{s1}\end{aligned}\right\} \tag{11}$$

3　算法设计及实例计算

3.1　算法设计

基于上述理论, 设计便于计算机处理的算法步骤描述如下.

步骤 1: 依据参数列表输入该坡口类型参数, 其中步骤 2 ~ 4 计算先焊面各焊层面积, 步骤 5 ~ 7 计算后焊面各焊层面积;

步骤 2: 输入先焊面各工序焊层厚度 $\Delta\delta_{fi}$, 初始化参数: $i = 1$, $\delta_{fi} = \Delta\delta_{fi}$;

若 $\delta_{fi} < R_1$, 按式(6) 计算 S_{fi}; 若 $\delta_{fi} \geqslant R_1$, 按式(7) 计算 S_{fi}; $\Delta S_{fi} = S_{fi}$; $i = i + 1$;

步骤 3: 如果 $i \leqslant n1$; $\delta_{fi} = \delta_{fi} + \Delta\delta_{fi}$;

若 $\delta_{fi} < R_1$, 按式(6) 计算 S_{fi}; 若 $\delta_{fi} \geqslant R_1$, 按式(7) 计算 S_{fi}; $\Delta S_{fi} = F_{fi}$; $i = i + 1$; 重复步骤 3;

如果 $i = n_1 + 1$; 转步骤 4;

步骤 4: 按式(3) 计算余高面积 S_{e1}, 并将计算面积加到第 n_1 层面积, 即 $\Delta S_{fn1} = \Delta S_{fn1} + S_{e1}$;

步骤 5: 输入后焊面各工序焊层厚度 $\Delta\delta_{si}$ ($i = 1, 2, \cdots n_2$), 计算背面清根面积 S_g, 并将清根面积加入后焊面第一层面积, 初始化参数: $i = 1$, $\delta_{si} = \Delta\delta_{si}$; 若 $\delta_{si} < R_2$, 按式(8) 计算 S_{si}; 若 $\delta_{si} \geqslant R_2$, 按式(9) 计算 S_{si}; $\Delta S_{si} = S_{si} + S_g$; $i = i + 1$;

步骤 6: 如果 $i \leqslant n_2$; $\delta_{si} = \delta_{si} + \Delta\delta_{si}$; 若 $\delta_{si} < R_2$, 按式(8) 计算 S_{si}; 若 $\delta_{si} \geqslant R_2$, 按式(9) 计算 S_{si}; $\Delta S_{si} = S_{si} + S_g$; $i = i + 1$; 重复步骤 6;

如果 $i = n_2 + 1$; 转步骤 7;

步骤 7: 按式(5) 计算余高面积 S_{e2}, 并将计算面积加到第 n_2 层面积, 即 $\Delta S_{sn2} = \Delta S_{sn2} + S_{e2}$;

在求出各焊层截面面积基础上, 按式(12) 求出各层理论焊缝熔敷金属量为

$$G_w = SL\rho/10^3 \tag{12}$$

式中: F 为焊缝横截面面积; L 为焊缝长度; ρ 为熔敷金属比重.

考虑到焊接过程损耗等因素, 实际焊材用量 G 的基本计算式为

$$G = G_w/\eta \cdot \Psi \tag{13}$$

式中: η 为焊接材料熔敷效率; Ψ 为焊材余量系数.

3.2　焊缝焊材用量计算实例

依据上述算法开发了焊材消耗用量计算模块, 该模块可以按焊接工序对不同种类、不同规格的焊材进行用量计算.

范例: 内直径为 2 000 mm 的压力容器筒体, 材料为 16MnR, 厚度 36 mm; 由三个 2 m 长的筒节组焊而成. 采用如图 4 所示尺寸的坡口, 坡口间隙 3 mm, A 面为先焊面, B 面为后焊面. 采用如下焊接工序进行.

先焊面工序一: 焊条电弧焊, 采用直径 4 mm 的 J507 焊条焊二层, 焊层厚度 5 mm; 工序二: 焊条电弧焊, 采用直径 5 mm 的 J507 焊条焊三层, 焊层厚 8 mm; 工序三: 采用埋弧自动焊焊丝为 H10Mn2, 焊剂为 SJ101 将坡口填满, 并盖面.

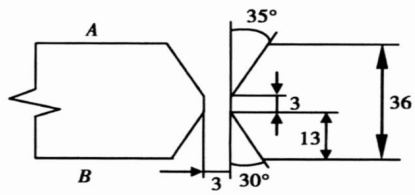

图 4　坡口参数图

Fig. 4　Parameters of groove

A 面焊缝余高 $e_1 = 4$ mm, 焊缝加宽 $a_1 = 4$ mm. B 面采用碳弧气刨清焊根并打磨, 清根深度 5 mm, 清根宽度 15 mm.

后焊面然后采用埋弧自动焊焊丝为 H10Mn2, 焊剂为 SJ101 填满坡口并盖面. B 面焊缝余高 3 mm, 焊缝加宽 4 mm. 焊条的熔敷效率为 $\eta = 50\%$, 焊丝的熔敷效率为 0.93, 熔敷金属的比重 $\rho = 7.85$ g/cm^3; 余量系数 $\Psi = 1.1$; 焊剂效率系数为 1.2 .

焊材用量计算工具界面如图 5 所示. 筒体纵环缝焊材消耗用量计算结果如表 1 所示.

在计算单个焊缝焊材消耗的基础上, 可以汇总整个产品的全部焊缝耗材定额, 做到领料有理, 回收有据, 同时可以依据焊材消耗计算焊接工时并进行汇总, 便于成本管理.

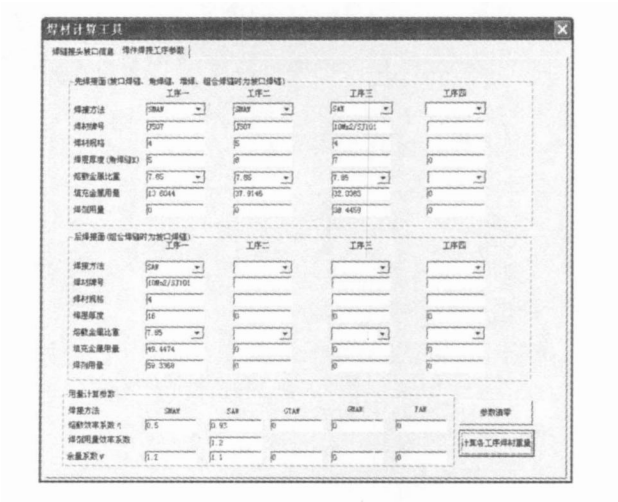

图 5 焊材消耗计算结果界面

Fig. 5 Interface of computing results

表 1 焊材消耗用量结果

Table 1 Results of welding material dosage

焊材名称	牌号	规格 ϕ/mm	用量 m/kg
焊条	J507	4	14
焊条	J507	5	38
焊丝	H10Mn2	4	82
焊剂	SJ101		100

4 结 论

(1) 在分析焊缝焊层截面面积理论基础上, 提出了多焊层焊缝截面面积求解算法, 有效解决了各工序焊材消耗用量计算, 改变传统粗放的计算模式.

(2) 在计算单个焊缝焊材消耗的基础上, 可以汇总整个产品的全部焊缝耗材定额, 做到领料有理, 回收有据, 同时可以依据焊材消耗计算焊接工时并进行汇总, 便于成本核算.

参考文献:

[1] 朱志明, 张崇柯, 陈丙森. 焊接结构件装焊 CAPP 系统的研究与开发[J]. 焊接学报, 2001, 22(4): 87—92.
Zhu Zhiming, Zhang Chongke, Chen Bingsen. Study and development of Assembly weldeding CAPP system for welded structures [J]. Transactions of the China Welding Institution, 2001, 22 (4): 87—92.

[2] 魏艳红. 焊接工艺文件管理与编制 [J]. 焊接, 1999, 23(10): 11—13.
Wei Yanhong. Management and preparation of welding document [J]. Welding and Joining, 1999, 23(10): 11—13.

[3] 钱晓军, 沈春龙, 王克鸿. 面向 WCAPP 的工艺数据处理[J]. 焊接学报, 2007, 28 (4): 53—57.
Qian Xiaojun, Shen Chunlong, Wang Kehong. Research on technology of processing of process data based on WCAPP[J]. Transactions of the China Welding Institution, 2007, 28 (4): 53—57.

作者简介: 沈春龙, 男, 1970 年出生, 博士, 副教授. 主要从事焊接 CAD/CAPP/CAM 应用软件开发, 图形图像工程等研究. 发表论文 30 余篇.

Email: shenchunlong@njnu.edu.cn

power supply, and a proper wave form control method was designed. The effects of different wave form control parameters on short circuit droplet transfer were studied by orthogonal experimental design and analysis of variance. Parameters were optimized on the basis of orthogonal experimental design and a stable short circuit droplet transfer and nice weld bead was obtained. The results prove that current rise speed on the beginning of short circuit and current falling speed during arc period have great effects on the stability of short circuit procedure. Current rise speed on the later period of short circuit has bigger effect on average time of arc period, and little effect on the stability of the period of short circuit.

Key words: short circuit transfer; orthogonal experiment; waveform control

Analyses of process of MIG droplet transfer with longitudinal magnetic CHANG Yunlong, LI Duo, LI Dayong, SHAO Liguang (School of Material Science and Engineering, Shenyang University of Technology, Shenyang 110023, China). p21—24

Abstract: When aluminum alloy was welded by metal inert-gas (MIG) welding with longitudinal intermittent alternative magnetic fields, a high-speed video camera was used to view the whole process of electrode melting, a droplet developing at the electrode end, the droplet detaching and transferring to the weld pool. And the difference between droplet transition with longitudinal magnetic and without longitudinal magnetic was analyzed. The experiment results indicate that there are obvious change in the metal transfer with longitudinal intermittent alternative magnetic fields, which the shape of droplet changes from globular without longitudinal magnetic to flat shape, and the droplets detach from the tip of the wire, diverge from the axial line of the wire and fall down with turning movement. With the same frequencies, droplet transition time ranges from 4.5 ms to 6 ms when excitatory current is smaller, but droplet transition time needed ranges from 5 ms to 15 ms when excitatory current is larger, so excitatory current has a large influence on droplet transfer.

Key words: longitudinal magnetic; metal inert-gas welding; high-speed video camera; droplet transfer.

Analyses on microstructure and mechanical properties of friction welded joint of dissimilar powder metallurgy tungsten alloy between 93W and 98W ZHOU Jun[1], QI Xiubin[1], QIN Guoliang[2], ZHAO Yushan[1] (1. Harbin Welding Institute, Harbin 150080, China; 2. School of Materials Science and Engineering, Shandong University, Jinan 250061, China). p25—28

Abstract: 93W tungsten alloy and 98W tungsten alloy have their respective advantages in properties, and it is necessary to develop the composite tungsten alloy based on 93W tungsten alloy and 98W tungsten alloy. 93W tungsten alloy and 98W alloy were welded by the HSMZ-10 friction welding machine developed by authors and with the optimized welding parameters. The mechanical properties and microstructure of the welded joint were tested and analyzed. The results indicate that the welded joint has good mechanical properties and no welding defects such as incomplete penetration. There is no composition homogenization between 93W tungsten alloy and 98W alloy, and the tensile strength of welded joint is higher than that of the base metals.

Key words: friction welding; microstructure; mechanical properties; 93W tungsten alloy; 98W tungsten alloy

Correlation of arc acoustic signals and droplet transfer in aluminum pulsed MIG welding SHI Yu[1], HUANG Jiankang[2], NIE Jing[2], FAN Ding[1] (1. Key Laboratory of Non-ferrous Metal Alloys and Processing of Ministry of Education, Lanzhou University of Technology, Lanzhou 730050, China; 2. State Key Laboratory of Gansu Advanced Non-ferrous Metal Materials, Lanzhou University of Technology, Lanzhou 730050, China). p29—32

Abstract: The correlation between arc acoustic signals and droplet transfer in aluminum pulsed MIG welding was studied. The arc sound signals under different droplet transfer were acquired by the designed experimental system and analyzed by using the methods of the wavelet de-noising, the power spectral density and the power spectral estimation of auto regressive and moving average. The analysis results show that the arc acoustic signals have different characters under short-circuit transfer, global transfer, projected droplet transfer and spray transfer, so the pattern of droplet transfer can be recognized by arc acoustic signals. These results have an industrial impact on controlling the stability of droplet transfer of aluminum pulsed MIG welding in real-time.

Key words: aluminum pulsed MIG welding; droplet transfer; arc acoustic signals; real-time detecting

Calculation of layered welding material dosage based on model of variant parameter groove SHEN Chunlong[1], QIAN Xiaojun[1], HUANG Youren[1], WANG Kehong[2] (1. Department Computer, Nanjing Normal University, Nanjing 210097, China; 2. Department Materials, Nanjing University Science and Technology, Nanjing 210094, China). p33—36

Abstract: Computing dissipative welding material dosage is an important content of welding procedure. The parameter model of normal groove type is unified by modifying parameters on basic of describing both-side double-U-groove parameters, which is easy to compute cross-section area of weld. By decomposing the cross-section of weld on the model, calculating complex area is predigested to computing area of some simple graphs. For getting dosage of welding material from each welding procedure, the cross-section area of corresponding welding layer should be obtained. An idea and theory of calculating welding layer cross-section on welding layer thickness are presented. The arithmetic of layered iterative calculation is designed and is realized in the software, which the usage of calculating tool is explained. By calculating material from a real groove, the result shows that precision and efficiency of computing dissipative welding

material are enhanced obviously.

Key words: welding material dosage; welding procedure; parameter model; area of welding layer

Vacuum diffusion welding of dissimilar materials of M2/40Cr

CHEN Chunhuan[1], ZHOU Yanbin[2], PAN Jinzhi[1], REN Ruiming[1], QI Zhengfeng[1] (1. School of Materials Science and Engineering, Dalian Jiaotong University, Dalian 116028, China; 2. Institute of Surface-Hardening Technique, DHI · DCW Group, Dalian 116041, China). p37—40

Abstract: The vacuum diffusion welding of high speed steel W6Mo5Cr4V2 (M2) with alloy structure steel 40Cr was studied by means of hardness test, tensile test, bending test, scanning electron microscope and OM analysis. Results show that sound metallurgical bonding is obtained between the two dissimilar materials at 1 100 ℃ for 30 minutes, which bonding pressure is 20 MPa and the vacuum level is not less than 0.1 Pa. The fractures of tensile test and bending test both take in place on the steel of 40Cr. So the strength of bonding zone is higher than 40Cr matrix. Ionnealing after quenching treatment at atrelatively lower temperature can ensure the required hardness of both the high speed steel and the structural alloy steel.

Key words: M2/40Cr dissimilar materials; vacuum diffusion welding; mechanical property; fracture morphology; microstructures

Study of tin whisker growth accelerated by rare earth Y

HAO Hu, LI Guangdong, SHI Yaowu, XIA Zhidong (School of Materials Science & Engineering, Beijing University of Technology, Beijing 100022, China). p41—44

Abstract: It is known that rare-earth elements exhibit high chemical activity and adding trace amount of rare-earth (RE) in the solder can significantly improve the properties of solder alloy. However, RE-phases with large size precipitated in the Sn-3.8Ag-0.7Cu-1.0 RE solder alloy are oxidized when exposed in air, tin whiskers growing rapidly on the surface of the oxidized RE-phases. Tin whisker growth on the surface of the oxidized YSn_3 phase is investigated at room temperature and 150 ℃ storage in air respectively. The results indicate that tin whiskers grow slowly and distribute unevenly on the surface of the oxidized YSn_3 phases during room temperature storage in air, but tin whiskers grow rapidly and the YSn_3 phase is extruded around even solder matrix during 150 ℃ storage in air.

Key words: lead-free solder; rare earth Y; tin whisker

Accuracy analysis and experimental method on three-dimensional information computing of weld seam

CHEN Xizhang[1], CHEN Shanben[2] (1. School of Material Science and Engineering, Jiangsu University, Zhenjiang 212013, China; 2. Institute of Welding Engineering, Shanghai Jiaotong University, Shanghai 200030, China). p45—48

Abstract: Binocular vision technology which simulates the function of the human eyes to observe the world is used to compute the three-dimensional information of weld seam in the welding field; two cameras as binocular vision are fixed on the end effecter of the welding robot. The accuracy analysis model of vision computing is constructed. The effect of vision system structure on vision computing, and the effect of the position of weld seam and the relative pose of weld seam between vision sensors on accuracy are analyzed. An experiment base on model theory is designed to validate the model analysis results, which show the correctness of the constructed model. The effects of repeatability positioning accuracy and TCP calibration error of welding robot for visual computing are also analyzed and tested. The results show that the effect of the former factor is not bigger than 0.3 mm, but the re-calibration is necessary when the calibrated error of TCP is bigger than 1 mm.

Key words: binocular vision; three-dimensional information; accuracy analysis; arc-welding robot

Fully digitalized control strategy of wire feed motor

SHA Deshang[1], LIAO Xiaozhong[1], SHAN Lijun[2], BAO Yunjie[2] (1. School of Automation, Beijing Institute of Technology, Beijing 100081, China; 2. Beijing Time Technology Company LTD, Beijing 100085, China). p49—52

Abstract: A fully digitalized control strategy consisting of the outer loop of rotating speed regulation and the inner loop of current regulation for wire feed motor is proposed. Variable parameter control method is implemented according to different working procedures of the wire feed motor. The power circuit of wire feeder is composed of buck converter and full-bridge inverter, and the operation principles of the power circuit are analyzed. Also plug braking is taken to improve the dynamic response of the proposed power circuit, and double loop-closed block is established. The good dynamic and static performance of the wire feed system with this control strategy is verified by experimental results.

Key words: wire feeding motor; gas metal arc welding; digitalization; double closed loop

Composite control of sliding mode and PI for inverter arc welding/cutting power supply

ZHU Guorong[1], QIAN Cuifeng[2], DUAN Shanxu[1], KANG Yong[1] (1. College of Electrical and Electronic Engineering, Huazhong University of Science and Technology, Wuhan 430074, China; 2. Valin Lianyuan Iron & Steel Thin Sheet Co. Ltd, Loudi 417009, China). p53—57

Abstract: According to the basic characteristics and the needs of arc welding/cutting power source, such as load current, short current and unload voltage, considering to the mains voltage fluctuation, economical and person security, the inverter arc welding/cutting power supply with composite control of sliding mode control (SMC) and PI is researched and designed. Through demonstrating the external characteristic demands of welding/cutting power supply and analyzing the control algorithm, PI control is used on current